Photonics and Nanostructures - Fundamentals and Applications 52 (2022) 101086

Contents lists available at ScienceDirect

Photonics and Nanostructures - Fundamentals and Applications

journal homepage: www.elsevier.com/locate/photonics

Cross-section mismatch: metamaterials to the rescue

Paulo Lourenço [a,b,*], Alessandro Fantoni [b], João Costa [b], Manuela Vieira [a,b]

[a] Departamento de Engenharia Eletrotécnica, Faculdade de Ciências e Tecnologia (FCT), Universidade Nova de Lisboa (UNL), Campus da Caparica, Faculdade de Ciências e Tecnologia, 2829-516 Caparica, Portugal

[b] ISEL/DEETC – Instituto Superior de Engenharia de Lisboa, Instituto Politécnico de Lisboa, Departamento de Engenharia Eletrónica e Telecomunicações e de Computadores, Rua Conselheiro Emídio Navarro, 1, 1959–007 Lisboa, Portugal

ARTICLE INFO

Keywords:
Metamaterial
Hexagonal lattice
Graded index waveguide
Subwavelength structures
Expanding/focusing light

ABSTRACT

Coupling light into and/or out of a photonic integrated circuit is often accomplished by establishing a vertical link between a single-mode optical fiber and a resonant waveguide grating, which is then followed by a tapered and a single-mode waveguides. The tapered waveguide operates as a spot-size converter, laterally expanding or contracting the light beam between the single-mode waveguide and the resonant waveguide grating. In this work, we propose using subwavelength structures to achieve tapering functionalities. To this end, we designed a metamaterial structure that enables the modulation of the refractive index necessary to either expand or focus a beam of light. Furthermore, we simulated the metamaterial structure through adequate numerical methods and the expanding, and focusing performances were analyzed in terms of efficiency and mode profile matching. We achieved over 43 % and 48 % for the integral overlap with the transverse magnetic fundamental mode for the focusing and expanding configurations, respectively, out of 49 % and 51 % of power transferred.

1. Introduction

Photonic integrated circuits usually require a structure to adapt the existing cross-section mismatch in waveguides of different dimensions. One such case is the vertical coupling of light between an optical fiber and a photonic integrated chip. For the outcoupling, the electromagnetic (EM) beam of energy diffracted by a resonant waveguide grating propagates in free space and toward a single-mode optical fiber, where it couples with its fundamental mode. For the incoupling, the beam of light coming from the optical fiber is diffracted by the resonant waveguide grating and couples with its fundamental mode. Either way, the grating structure must be wide enough to ensure efficient coupling with the mode of the optical fiber. Typical core widths are approximately 10 and 5 μm for single-mode optical fibers operating in the near infrared and visible wavelengths, respectively. Thus, these grating structures must be wider than the corresponding core width to couple the fundamental mode of the resonant waveguide grating with the lowest order mode of the optical fiber. Furthermore, the optical interconnects linking operational structures within the photonic integrated circuit are usually single-mode waveguides, 400–500 nm wide. So, a spot-size conversion is necessary between the mode profiles of the single-mode waveguide and the resonant waveguide grating.

Over the last two decades, a less conventional type of cross-section mismatch adapter has been reported – the denominated non-adiabatic taper. Examples of such structures were reported by Spühler [1] and Luyssaert [2] who, by exploiting the developments in genetic algorithms, announced highly efficient and compact non-adiabatic taper waveguides. Zhang [3] and Liu [4] used a similar strategy to design their compact tapers. The former exploited the effective medium theory to place a row of inclusions of a different material in a linear taper waveguide and numerically demonstrated the contraction of the EM beam within a short distance. The latter, again by placing inclusions along the sides and in the core of the propagating structure, obtained a compact staircase-like taper and a rectangular metamaterial waveguide with perturbations of the core refractive index at locations calculated by an evolutionary algorithm. Finally, Huang [5] explored the graded index (GRIN) concept by designing a structure consisting of several layers of alternating materials of different thicknesses, creating a material with a parabolic refractive index profile along the height of the structure. Our proposed line of action considers a similar approach, only creating a specific refractive index profile over the width of the structure instead of along its thickness.

* Corresponding author at: Departamento de Engenharia Eletrotécnica, Faculdade de Ciências e Tecnologia (FCT), Universidade Nova de Lisboa (UNL), Campus da Caparica, Faculdade de Ciências e Tecnologia, 2829-516 Caparica, Portugal.
E-mail address: pj.lourenco@campus.fct.unl.pt (P. Lourenço).

https://doi.org/10.1016/j.photonics.2022.101086
Received 30 January 2022; Received in revised form 12 July 2022; Accepted 21 October 2022
Available online 22 October 2022

The GRIN acronym is used to describe an inhomogeneous medium where the refractive index varies from one point to the next. There are three basic types of inhomogeneous media [6]:

- Axial GRIN, where the refractive index varies along the optical axis of the medium;
- Radial GRIN, where the refractive index varies from the optical axis to the edges of the structure;
- Spherical GRIN, which may be thought of as a symmetric index around a point, resulting in concentric spheres of constant refractive index.

In a GRIN material, the optical rays follow a curved path which, by proper selection of the refractive index, may have the same effect on light rays as a lens or a prism. Research regarding the use of GRIN media for optical applications in the macroscopic world has been conducted for many years now, with Maxwell being one of the first scientists to examine it using his own fisheye lens [7], which consisted of a spherical gradient medium able to focus, at the conjugate points relative to its center, rays of light emanating from points within or at the surface of the lens. In this work, the proposed structure consists of a GRIN waveguide wherein the refractive index varies only along the X-axis. This simpler GRIN structure has been accomplished by engineering a metamaterial region in the wider section waveguide (Fig. 1). The intended variation of the refractive index was obtained by embedding a lattice of SiO_2 cylinders in the Si_3N_4 core waveguide. As such, the resulting effective refractive index of the metamaterial is controlled through the radius of its cylindrical inclusions. This enabled the creation of a waveguide with a discrete Gaussian modulated distribution of the refractive index along the X-axis, similar to that previously developed [5], only with the variation of the refractive index along the width instead of the height of the core waveguide.

The object of interest of our research is shown as a 3D representation (Fig. 1). Although there are two objects represented, Fig. 1.a) and b) refer to the same structure, where one is the rotated image of the other. The former shows the structure configuration to perform the focusing functionality over the propagating light beam and the latter the expanding one. In both structures the input field is symbolized by the orange rectangles and the detecting monitors are represented by the green objects. This is a Si_3N_4 structure (brown objects) surrounded by SiO_2 (light blue object). The darker blueish region results from the cylindrical inclusions of different radii embedded in the core waveguide. These inclusions are disposed in a hexagonal lattice, enabling the structure to perform as a spot-size converter.

2. Materials and methods

This work presents the results obtained by simulation of a metamaterial structure performing as a focusing or expanding field waveguide for the transverse magnetic (TM) fundamental mode (the major component of the electric field is along the Y-axis). This structure is designed to operate at the 650-nm wavelength to comply with the PIX4life and PIXAPP pilot lines [8] under a multi-project wafer, and targeting the somewhat recent interest of life sciences in photonic structures, driven mostly by biosensing and biomedical applications [9–14]. The simulations are conducted in the software platform RSoft [15], making use of the packages implementing the beam propagation method (BPM) and the finite-difference time domain (FDTD) algorithm. To perform as a field expander, the involved structures are required to operate the lateral expansion of the propagating mode fields between two waveguides of different cross-sections, within the shortest possible length. To accomplish this, we start by generating a generic Gaussian function with a normal distribution as represented in Fig. 2.a). Next, we design a Si_3N_4 rectangular waveguide 12.35-μm wide and 150-nm thick, surrounded by air, and with a refractive index modulated by the generated Gaussian distribution. The resulting refractive index profile is presented in Fig. 2.b).

The proposed spot-size conversion functionality is based on the same principle that governs macroscopic optical lenses. By creating dissimilar optical paths for the wave fronts associated with rays of a beam of EM energy, it is possible to create diverging or converging beams of energy. A structure designed to converge wave fronts should be able to cancel out the natural divergence verified in a propagating mode when it crosses an interface to a wider section. Previous assumptions and the research developed by Safaai-jazi [16] have led to our work involving the GRIN waveguide. Although Safaai-jazi's work is based on a ray analysis, he was able to demonstrate that ray paths may be described by modulated sinusoidal functions, decreasing in period and amplitude, and with a gradual concentration of power from the larger to the smaller areas, while propagating through a GRIN medium.

So, we initiated this work by considering a rectangular cuboid waveguide with a refractive index profile modulated to enable field

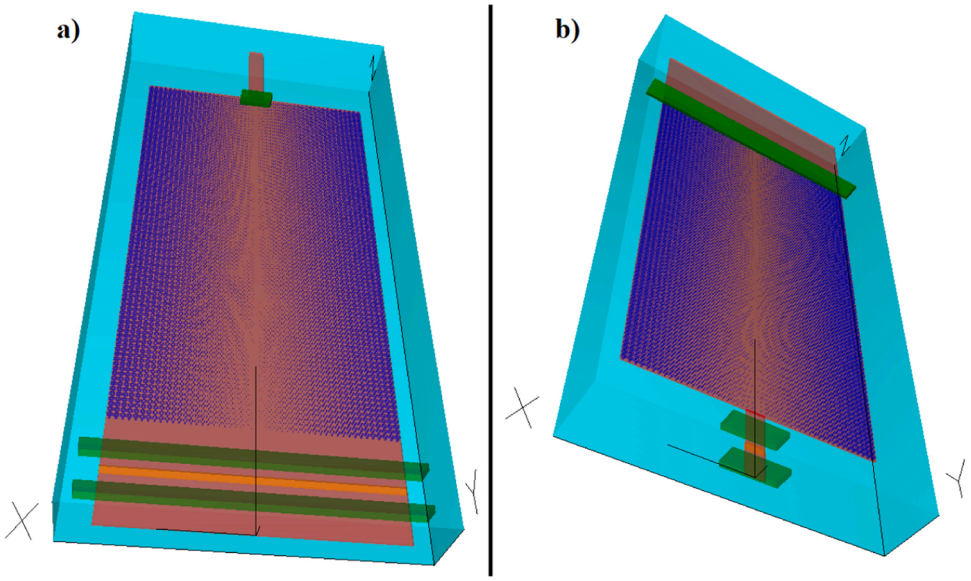

Fig. 1. Spot-size converter where the green objects are the detecting monitors, the orange rectangle is the launch field and the dark blueish region is the metamaterial section: (a) focusing and (b) expanding configurations.

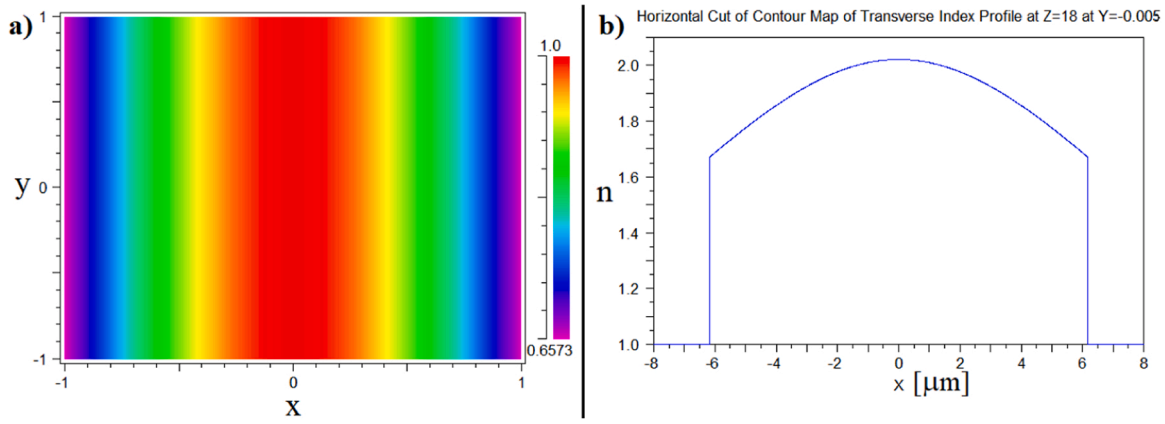

Fig. 2. Representation of the Gaussian modulated refractive index: (a) colormap representation of the Gaussian function (color bar represents the normalized value) and (b) Gaussian distribution of the refractive index of a Si_3N_4 waveguide surrounded by air.

expanding capabilities over a beam of EM energy. For the proof of concept of our proposal, we start by designing a structure consisting of a wider than thick Si_3N_4 input waveguide (1 μm × 0.15 μm), followed by a much wider cross-section waveguide (12.35 μm × 0.15 μm). The latter section is designed such that, right after the input waveguide and up to a given length, there is a region where the refractive index is modulated by the Gaussian function of Fig. 2.a). Then, this structure is terminated by a Si_3N_4 waveguide with the same cross-section as the previous region, and the whole structure is surrounded by a SiO_2 medium. At the top, the refractive index distribution of the designed structure and, at the bottom, a cut plane of the refractive index profile at Z = 20 μm are shown in Fig. 3.a). The next step consists of dividing the region where the refractive index is modulated by the Gaussian function into 51 slots of equal width (237.5 nm), and setting each slot with the corresponding value of the refractive index. This is presented in the upper part of Fig. 3. b), and the bottom part shows a cut plane of the designed refractive index profile at Z = 20 μm.

To independently engineer the refractive indices of each of the 51 slots, a metamaterial is used. The effective refractive index of each slot may be engineered by a hexagonal lattice of subwavelength cylindrical inclusions of a different material embedded in the medium of the slot. Moreover, the effective refractive index of each slot depends on the filling factor of the cylindrical inclusions, which can be calculated based on the effective medium approximation through Eq. (1) [17]:

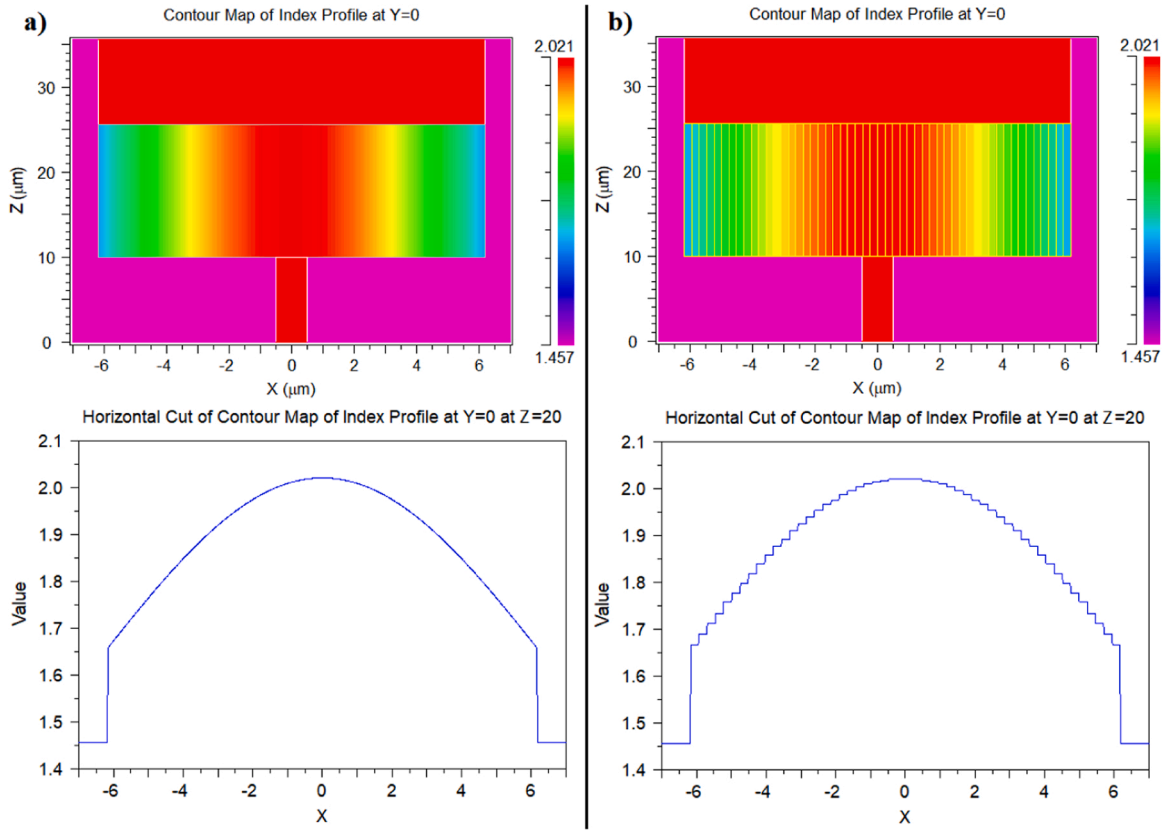

Fig. 3. Refractive index profiles (color bars refer to maximum and minimum values): (a) Gaussian distribution profile embedded in the Si_3N_4 waveguide and (b) Gaussian profile discretized over 51 slots.

$$f = \frac{(n_{core}^2 + n_{hole}^2)(n_{core}^2 - n_{eff}^2)}{(n_{core}^2 - n_{hole}^2)(n_{core}^2 + n_{eff}^2)} \quad (1)$$

where f is the filling factor, n_{core} is the refractive index of the core waveguide, n_{hole} is the refractive index of the cylindrical inclusions, and n_{eff} is the effective refractive index. Furthermore, when considering a hexagonal lattice inscribed in a slab segment of width d_0, and with a lattice constant of $a = 2/3d_0$, the diameter D of the cylindrical inclusions is given by Eq. (2):

$$D = d_0\sqrt{\frac{8}{3\sqrt{3}\pi}f} = 0.70005 d_0\sqrt{f} \quad (2)$$

Our simulation platform [15] offers the possibility of generating dynamically-sized arrays with a given lattice, width, and length. Using Eqs. (1) and (2) allows engineering a metamaterial with a hexagonal lattice structure for each of the discretized slots. The resulting structure is 13.85-μm wide and 24-μm long (Fig. 4, insets show details of cylindrical inclusions of the hexagonal lattice). The final width and length of the structure are found through simulations where these parameters are iterated and the optimal values selected. The radius of the inclusions varies in a way to implement the modulation of the refractive index profile along the width of the structure. This modulation enables control of the beam divergence, transforming the propagating fields in a collimated wave with the phase front confined within the boundaries of the waveguide and presenting a profile that matches well with the fundamental mode.

3. Simulations and results

The structure in Fig. 3.b) is simulated with the BPM to evaluate the spot-size conversion capabilities. Although we conduct 3D full-vectorial BPM simulations, the solution for the propagating fields provided by this method does not consider reflections. In fact, we could account for reflections if using FDTD to simulate and obtain the fields near the geometric interfaces, and then propagating these fields back and forth with BPM. For the evaluation of the spot-size conversion functionality and because the final simulations will be conducted with the FDTD algorithm, the BPM is sufficient for now. The results obtained in this simulation show the spot-size conversion functionality (Fig. 5) and we can also verify that the field profile of the propagating mode is preserved throughout the propagation path. The relevant simulation parameters are:

- Simulation type: 3D full-vectorial BPM;
- Polarization: TM;
- Input field: fundamental mode;
- Input waveguide (cross-section): 1 μm × 0.15 μm;
- Output waveguide (cross-section): 12.35 μm × 0.15 μm;
- Grid size (X, Y, Z): 0.01 μm, 0.01 μm, 0.02 μm (default values);
- GRIN profile length: 17.6 μm.

Previous simulation agrees with our proposed functionality – a discretized GRIN profile may be used to converge wavefronts, similarly to the operation of macroscopic lenses. In photonics, this functionality is usually performed by taper waveguides, but these are long structures of several hundreds of micrometers. Remarkably, the length of the metamaterial planar waveguide in previous BPM simulation is less than 20 μm. We further investigate and confirm this behavior using a set of simulations implementing the FDTD algorithm. This algorithm returns the exact field solutions by solving Maxwell's equations with no approximations. All discrete refractive index slots in previous structures are replaced by the corresponding metamaterial segment (a dynamic array of cylindrical inclusions generated with our software platform) and the simulation is executed with the following relevant parameters:

- Simulation type: 3D FDTD;
- Polarization: TM;
- Input field: fundamental mode;
- Input waveguide (cross-section): 1 μm × 0.15 μm;
- Output waveguide (cross-section): 13.85 μm × 0.15 μm;
- Grid size (X, Y, Z): 0.01 μm, 0.1/0.01 μm (non-uniform grid), 0.01 μm;
- GRIN profile length: 24 μm;
- Boundary conditions (min/max): X(Symmetric/PML), Y(PML/PML), Z(PML/PML).

Evolution of the electric field while it propagates throughout the structure is shown in Fig. 6.c). It is evident the transformation operated by the metamaterial structure over the propagating wave front, approximating it to a collimated beam delimited by the boundaries of the waveguide. Furthermore, we show the monitored quantities at locations of interest (Fig. 6.a)), i.e., the overlap integral of the propagating field with the TM_0 mode, and the reflected, transmitted, and input powers. The electric field profile of E_y obtained at the end of the GRIN region is shown in Fig. 6.b). The relevant metrics for Fig. 6 are:

- Only approximately 53.4 % of the power present in the launch field is coupled into the structure (light blue line in Fig. 6.a));
- Over 51.8 % of the propagated power reaches the end detector (red line in Fig. 6.a);
- Overlap integral of the propagated fields with the fundamental mode of the waveguide (TM_0) achieves over 48.1 % (blue line in Fig. 6.a));
- Just over 2.3 % of reflected power is detected (green line in Fig. 6.a)).

Next, we further investigate the possibility of this structure being

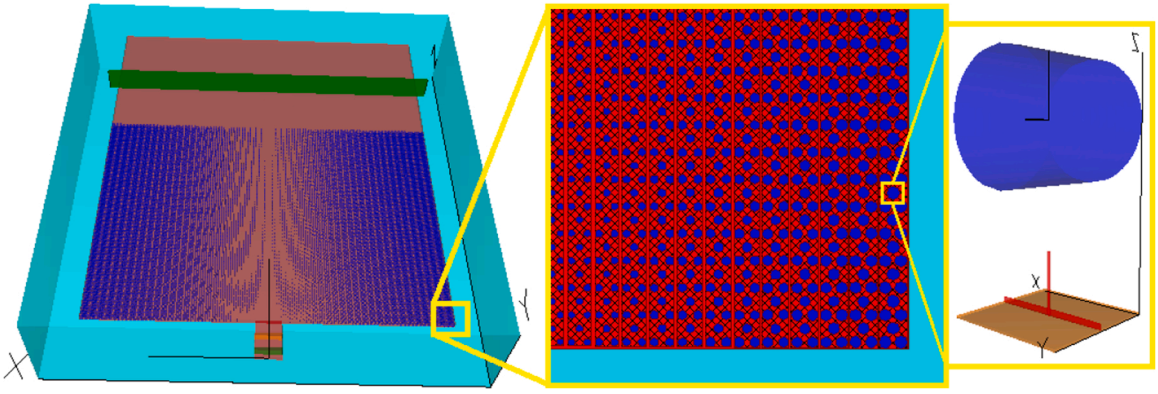

Fig. 4. Implemented hexagonal lattice in the waveguide (green and orange objects are field monitors and input field, respectively). The insets show details of the hexagonal lattice structure and of the cylindrical inclusions (brown plane with the red fixture symbolizes the incoming wave front).

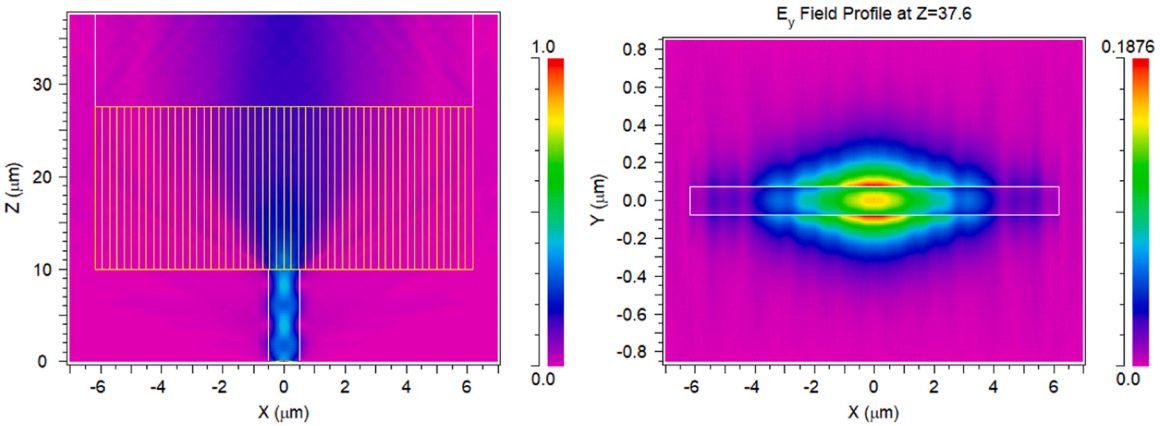

Fig. 5. Wavefront converging capability: (left) TM_0 propagation in the X–Z plane and (right) electric field collected at the end of the structure.

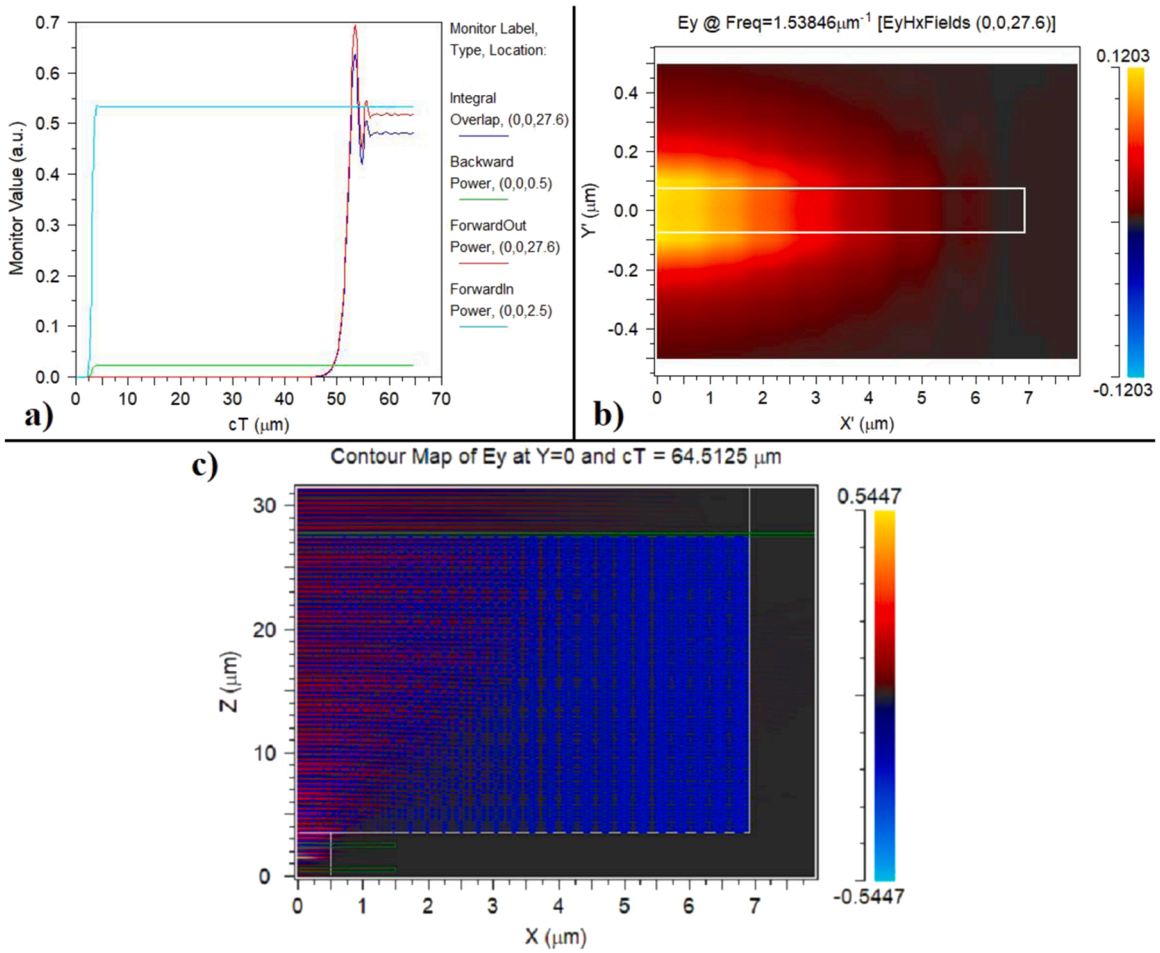

Fig. 6. Field propagation along the structure: (a) propagation parameters monitored – integral overlap with TM_0 (blue line), reflected power detected at Z = 0.5 μm (green line), transmitted power at Z = 27.6 μm (ForwardOut – red line), and input power at Z = 2.5 μm (ForwardIn – light blue line); (b) transverse profile of E_y monitored at the end of the GRIN region (Z = 27.6 μm); and (c) E_y propagation showing gradual cancellation of the beam's divergence (color bar refers to instantaneous field amplitude in Vm^{-1}).

able to operate the opposite way, i.e. instead of expanding the field, being able to focus the EM fields propagating from a wide into a narrower waveguide. To this end, we rotate the whole structure 180°, rearrange the locations of all detecting monitors, use the fundamental mode (still TM_0) of the wider waveguide as the input field, and the simulation is carried out with the same relevant parameters as before. The results are presented in Fig. 7, and the relevant metrics are:

- Only approximately 49.5 % of the power present in the launch field is coupled into the structure (green line in Fig. 7.a));
- Just below 45.6 % of the propagated power reaches the end detector (red line in Fig. 7.a));
- Overlap integral of the propagated fields with the fundamental mode of the waveguide (TM_0) achieves just over 43.6 % (blue line in Fig. 7.a));

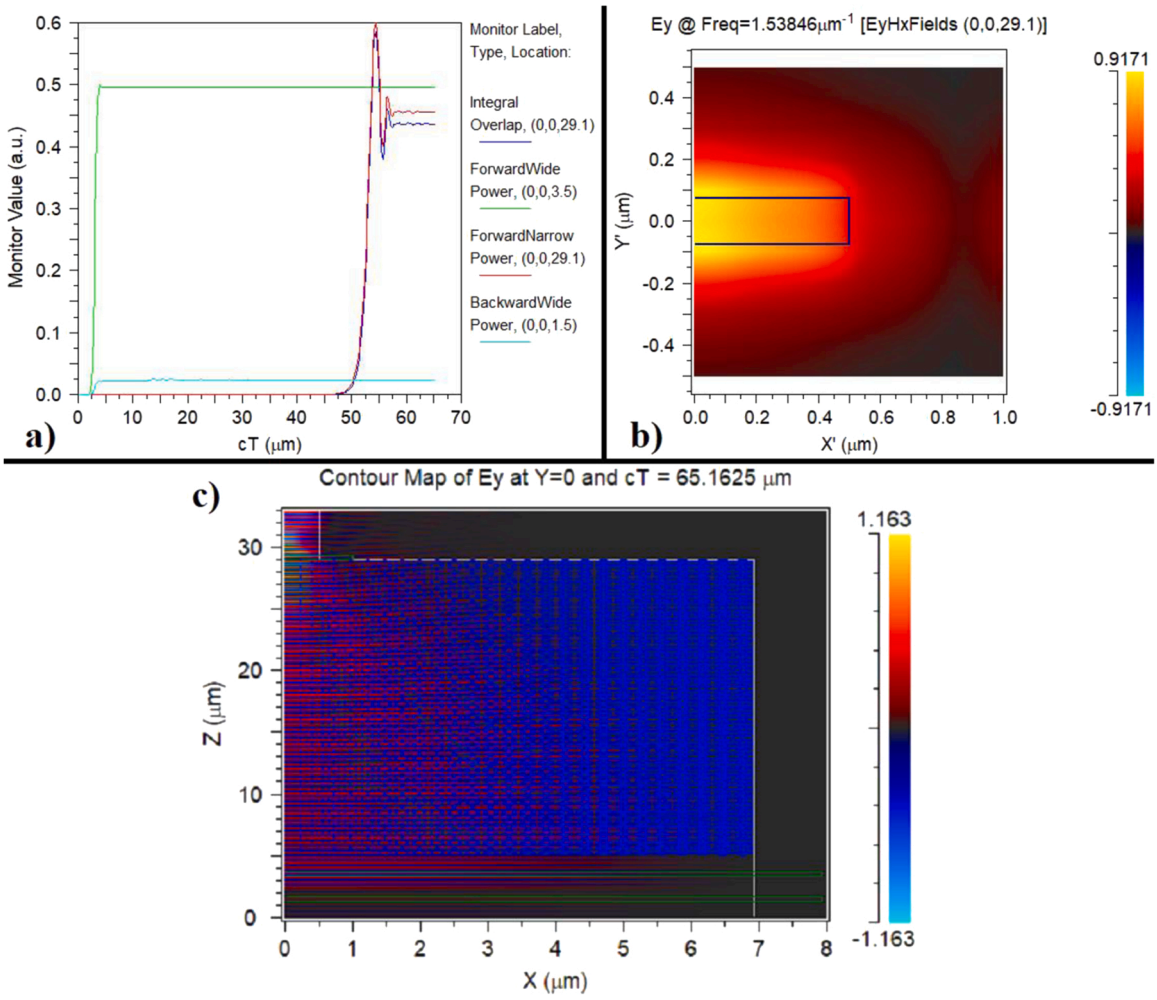

Fig. 7. Propagation of fields along the structure: (a) propagation parameters monitored – integral overlap with TM_0 at Z = 29.1 μm (blue line), transmitted power at Z = 29.1 μm (ForwardNarrow – red line), and input power at Z = 2.5 μm (ForwardWide – green line); (b) transverse profile of Ey monitored in the narrower waveguide (Z = 29.1 μm); and (c) E_y propagation showing gradual focusing of the EM beam (color bar refers to instantaneous field amplitude in Vm^{-1}).

- Less than 2.4 % of reflected power is detected (green line in Fig. 7. a)).

4. Discussion

In this work, we design and simulate a structure that uses a metamaterial to operate as a beam expander or concentrator. To accomplish this, cylindrical inclusions of a lower refractive index material are embedded in a rectangular cuboid waveguide. These are subwavelength inclusions in a hexagonal lattice, hence the intended refractive index may be obtained by the effective medium approximation for a given inclusion radius. By embedding cylindrical inclusions with varying radii in a hexagonal lattice, we can control the refractive index of the structure along the X-axis and modulate it with a Gaussian profile.

The results in our FDTD simulations are quite promising. Not only do we observe expansion of the TM fundamental mode, but the focusing functionality is also verified if the structure operates in the opposite way. In both functionalities we can achieve over 49 % of power transferred into the end waveguide, an integral overlap with the TM fundamental mode of over 43 % and less than 2.4 % of reflected power. A note worth of mentioning, although outside the scope of this work, is the difference in power amplitude verified between the launch and the propagating fields in the beginning of the simulation – one should observe that these simulations consider as input an electric field polarized along the Y-axis to excite the fundamental mode of the structure, while there is a geometric constraint (the thickness of the waveguide) on the same axis. This excites a stationary wave (TM_0) that results from two interfering waves, each bouncing off either the top or the lower walls of the waveguide, and as a result the power amplitude verified in our simulations (approximately 3 dB lower than the launch field, in this case). As such, we demonstrate the structure's capability to excite the TM_0 mode and also obtain the propagation results through simulation. Finally, we present in Table 1 a summary of the relevant parameters and the corresponding results, collected in the simulations of both functionalities.

Further work will consist of investigating the applicability of these structures in different wavelength ranges and the TE polarization, and the fabrication of a physical prototype to verify these simulation results.

Table 1
Results and relevant parameters for the GRIN planar waveguide.

	Power transfer	Overlap integral	Backward power	Taper length	Taper width
Fields expansion	0.5183	0.4818	0.0231	24 μm	13.85 μm
Fields focusing	0.4954	0.4366	0.0237	24 μm	13.85 μm

Funding

This research was supported by EU funds through the FEDER European Regional Development Fund (project LISBOA-02–0145-FEDER-031311) and by Portuguese national funds by FCT – Fundaç ão para a Ciência e a Tecnologia through grant SFRH/BD/144833/2019 and projects PTDC/NAN-OPT/31311/2017 and UIDB/00066/2020, and by Instituto Politécnico de Lisboa with projects IPL/2021/wavesensor_ISEL and IPL/2021/MuMIA2D.

Declaration of Competing Interest

The authors declare that they have no known competing financial interests or personal relationships that could have appeared to influence the work reported in this paper.

References

[1] M.M. Spuhler, B.J. Offrein, G.-L. Bona, R. Germann, I. Massarek, D. Erni, A very short planar silica spot-size converter using a nonperiodic segmented waveguide, J. Light. Technol. 16 (1998) 1680–1685, https://doi.org/10.1109/50.712252.

[2] B. Luyssaert, P. Bienstman, P. Vandersteegen, P. Dumon, R. Baets, Efficient nonadiabatic planar waveguide tapers, J. Light. Technol. 23 (2005) 2462–2468, https://doi.org/10.1109/JLT.2005.850795.

[3] J. Zhang, J. Yang, H. Xin, J. Huang, D. Chen, Z. Zhaojian, Ultrashort and efficient adiabatic waveguide taper based on thin flat focusing lenses, Opt. Express 25 (2017) 19894–19903, https://doi.org/10.1364/oe.25.019894.

[4] Y. Liu, W. Sun, H. Xie, N. Zhang, K. Xu, Y. Yao, S. Xiao, Q. Song, Adiabatic and ultracompact waveguide tapers based on digital metamaterials, IEEE J. Sel. Top. Quantum Electron. 25 (2018), 4700106-6, https://doi.org/10.1109/JSTQE.2018.2846046.

[5] Y. Huang, S.-T. Ho, Superhigh numerical aperture (NA > 1.5) micro gradient-index lens based on a dual-material approach, Opt. Lett. 30 (2005), https://doi.org/10.1364/OL.30.001291.

[6] C. Gomez-Reino, M.V. Perez, C. Bao, Gradient-Index Optics, Springer, Berlin Heidelberg, 2002.

[7] E. Marchand, Gradient Index Optics, Academic Press, 1978.

[8] H. Jans, P. O'Brien, I. Artundo, M.A.G. Porcel, R. Hoofman, D. Geuzebroek, P. Dumon, M. van der Vliet, J. Witzens, E. Bourguignon, P. Van Dorpe, L. Lagae, Integrated bio-photonics to revolutionize health care enabled through PIX4life and PIXAPP, SPIE, Nanoscale Imaging, Sensing, and Actuation for Biomedical Applications XV, Feb. 2018, p. 31, doi: 10.1117/12.2288519.

[9] M.A. Cooper, Optical biosensors: where next and how soon, Drug Discov. Today 11 (2006) 1061–1067, https://doi.org/10.1016/j.drudis.2006.10.003.

[10] Y. Fang, Label-free cell-based assays with optical biosensors in drug discovery, Assay. Drug Dev. Technol. 4 (2006) 583–595, https://doi.org/10.1089/adt.2006.4.583.

[11] A. Fernández Gavela, D. Grajales García, J. Ramirez, L. Lechuga, Last advances in silicon-based optical biosensors, Sensors 16 (2016) 285, https://doi.org/10.3390/s16030285.

[12] M. Paulsen, S. Jahns, M. Gerken, Intensity-based readout of resonant-waveguide grating biosensors: systems and nanostructures, Photon. Nanostruct. 26 (2017) 69–79, https://doi.org/10.1016/j.photonics.2017.07.003.

[13] P. Lourenço, A. Fantoni, M. Vieira, Simulation analysis of a thin film semiconductor MMI 3dB splitter operating in the visible range, In: Proceedings of the Fourth International Conference on Applications of Optics and Photonics, Oct. 2019, p. 4, doi: 10.1117/12.2526656.

[14] J. Costa, A. Fantoni, P. Lourenço, M. Vieira, Simulation of a parallel waveguide array structure suitable for interrogation scheme in a plasmonic biosensor, In: Proceedings of the Physics and Simulation of Optoelectronic Devices XXVIII, 2020, 112742B, 83. doi: 10.1117/12.2546178.

[15] RSoft, Synopsys R.Soft Solutions. ⟨https://www.synopsys.com/optical-⟩solutions/rsoft.html (accessed July 10, 2021).

[16] A. Safaai-jazi, Propagation properties of tapered graded-index waveguides, J. Mod. Opt. 43 (1996) 1921–1932, https://doi.org/10.1080/09500349608232860.

[17] D. Gao, Z. Zhou, Nonlinear equation method for band structure calculations of photonic crystal slabs, Appl. Phys. Lett. 88 (2006), 163105, https://doi.org/10.1063/1.2194887.